Comparison of Dispersion Model of Magneto-Acoustic Cyclotron Instability with Experimental Observation of ^{3}He Ion Cyclotron Emission on JT-60U

Shuhei Sumida[1]*, Kouji Shinohara[2], Ryuya Ikezoe[1], Makoto Ichimura[1], Mizuki Sakamoto[1], Mafumi Hirata[1], and Shunsuke Ide[2]

[1]*Plasma Research Center, University of Tsukuba, Tsukuba, Ibaraki 305-8577, Japan*
[2]*National Institutes for Quantum and Radiological Science and Technology, Naka, Ibaraki 311-0193, Japan*

The Magneto-acoustic Cyclotron Instability (MCI) is a possible emission mechanism for Ion Cyclotron Emissions (ICEs). A dispersion model of the MCI driven by a drifting-ring-type ion velocity distribution has been proposed. In this study, the model was compared with the experimental observations of ^{3}He ICEs (ICEs(^{3}He)) on JT-60U. For this purpose, at first, velocity distributions of deuterium-deuterium fusion produced fast ^{3}He ions at the time of an appearance of the ICE(^{3}He) were evaluated by using a fast ion orbit following code under a realistic condition. The calculated distribution at the edge of the plasma on the midplane on the low field side is shown to have an inverted population and strong anisotropy. This distribution can be reasonably approximated by the drifting-ring-type distribution. Next, dispersions of the MCIs driven by the drifting-ring-type distribution were compared with those of observed ICEs(^{3}He). The comparison shows that toroidal wavenumbers and frequencies of the calculated MCIs agree with those of the observed ICEs(^{3}He).

1. Introduction

Alfvén waves in the ion cyclotron range of frequency (ICRF) can be excited by non-thermal ion distributions. Ion Cyclotron Emissions (ICEs) are the excited Alfvén waves and thought to be driven by fast ions originated from neutral beams (NBs) and fusion reactions. The ICEs are often observed in the frequency range near a fundamental cyclotron frequency for the fast ion and its higher harmonics at the edge of the plasma on the midplane on the low field side, and have been detected in several tokamak and helical devices.[1-8] The Magneto-acoustic Cyclotron Instability (MCI) is a possible emission mechanism for the ICE and Doppler-shifted ion cyclotron resonance condition is the key to the excitation of the MCI according to linear analytical theory and non-linear particle simulations.[9-16]

The MCI is driven by inverted and anisotropic velocity distribution of the fast ions. A formation process of the inverted and anisotropic distribution of the fusion produced fast ions is considered as follows. The fusion produced ions are generated mainly in the core region of the plasma. The fusion produced ions with pitch angles near the passing-trapped boundary draw large trajectories. The trajectories range from the core region to the edge of the plasma on the midplane on the low field side due to their high energies of MeV orders (see Fig. 8 as an example). The trajectory scales become small and the fast ions do not reach the plasma edge when they are decelerated due to ion-electron collisions near the core region. As a result, the population of the fast ions having the relatively low energy becomes less at the plasma edge. Namely, the fast ion distribution there has a positive gradient in the coordinate of the energy (the inverted population) and strong pitch-angle anisotropy. The emission mechanism for the ICE is thought to be the MCI driven by this inverted and anisotropic distribution. The above excitation process of the ICE is indirectly supported by the experimental observations that the frequencies of the ICEs are close to the ion cyclotron frequencies at the plasma edge, and that there is a correlation between the ICEs and edge localized modes.[1-8]

In the theoretical analysis, the inverted and anisotropic distribution at the plasma edge is often approximated by a drifting-ring-type ion velocity distribution.[11-16] We introduce one of the drifting-ring-type distribution functions. It is expressed by a Gaussian in the parallel direction and a delta function in the perpendicular direction to the magnetic field. Namely, it is given by,

$$f = \frac{1}{2\pi^{3/2} u v_{\|s}} \exp\left[-\frac{(v_{\|} - v_{\|c})^2}{v_{\|s}^2} \right] \delta(v_{\perp} - u) \cdot \qquad (1)$$

where $v_{||}$ and $v_{\perp}$ are parallel and perpendicular velocity components to the magnetic field,

respectively. $v_{||c}$ is the center of the Gaussian of the parallel speed, $v_{||s}$ is its spread and u is the perpendicular velocity of the fast ions. A dispersion model of the MCI driven by the drifting-ring-type distribution has been proposed from several reports where the frequency based on the model is comparable to the experimental observation of the ICE and there is a closely proportional relation between the linear growth rate based on the model and the observed ICE amplitude.[2,3,12] In order to assess this kind of dispersion model properly, it is important to evaluate its wavenumber on the basis of experimental observations in addition to the frequency. However, works on a comparison of the wavenumber based on the proposed model with that of the observed ICE are not reported so far. On JT-60U, quantitative measurements of the toroidal wavenumber of the ICEs have been carried out.[5-7] Not only the frequency, but also the toroidal wavenumber based on the dispersion model can be compared with the experimental observation of the ICE on JT-60U.

On JT-60U, the ICE thought to be driven by the fast D ions originated from the NB injection (ICE(D)) was observed. In addition, the ICEs related to the deuterium-deuterium (DD) fusion produced ^{3}He (ICE(^{3}He)), H (ICE(H)), and T ions (ICE(T)) were detected.[4-7] In this paper, we focused on the ICE(^{3}He) and compared the toroidal wavenumber and the frequencies based on the proposed dispersion model with those observed in the experiments on JT-60U. For the purpose, at first, we evaluated the velocity distribution of the DD fusion produced fast ^{3}He ions at the time of an appearance of the ICE(^{3}He). This evaluation is carried out by using the orbit-following Monte-Carlo (OFMC) code[17] under a realistic condition where plasma parameters measured in the experiments and collisional effects are taken into account. The results show that the calculated distribution at the plasma edge has the inverted population and the strong anisotropy, and can be reasonably approximated by the drifting-ring-type distribution. Next, we compared the dispersions of the MCIs driven by the drifting-ring-type distribution with those of the observed ICEs(^{3}He). The comparison shows that the proposed dispersion model is consistent with the experimental observation of the ICE(^{3}He).

This paper is organized as follows. We introduce the experimental setup in section 2. The velocity distributions of the DD fusion produced fast ^{3}He ions are evaluated by using the OFMC code under the realistic condition in section 3. In section 4, we describe the comparison of the dispersion based on the model with the experimental observation of the ICE(^{3}He). We summarize this paper in section 5.

2. Experimental setup

Positive ion-based NBs were injected in the both almost perpendicular (perp. P-NBs) and tangential (tang. P-NBs) directions to the toroidal magnetic field in JT-60U. A typical beam acceleration voltage E_{AC} of the P-NBs was ~80 kV. We measured electrostatic and electromagnetic fluctuations with ICRF antennas used as multiple pick-up loops.[5-7] Figure 1 shows a schematic drawing of the ICRF antennas which were located on the first wall on the low field side. Two antenna straps and four antenna straps are arranged in the poloidal and toroidal directions, respectively. Dividing phase differences of the fluctuations by distances between the multiple antenna straps, we obtained their wavenumbers. We used #1, #4 and #5 antenna straps for measuring the toroidal wavenumbers. The distance of the antenna straps between #1 and #4 is 0.44 m and that between #4 and #5 is 1.23 m. We recorded the signals by the sampling frequency of 500 MSamples/sec during 100 μsec in every 50 msec.

3. Evaluation of velocity distribution of DD fusion produced fast ^{3}He ions

3.1 Observation of ICE(^{3}He) in almost stationary plasmas

We evaluated the velocity distribution of the DD fusion produced fast ^{3}He ions in a stationary phase to collect good statistics in the orbit calculation. Figure 2 shows the temporal evolution of (a) a plasma current I_{P}, (b) a safety factor at 95% of the magnetic flux q_{95}, and (c) a major radial position of the edge of the plasma on the midplane on the low field side R_{edge} in the discharge of E48461. The I_{P} and the q_{95} become almost constant after t = ~2.5 sec. Then, the R_{edge} also becomes constant after t = ~4.0 sec. Namely, the plasma equilibrium becomes stationary after t = ~4.0 sec. Figure 2 shows (d) NB powers P_{NB} of the perp. P-NB (solid line) and the tang. P-NB (dotted line), (e) a line-averaged density $\bar{n}_{\mathrm{e}}$, (f) a stored energy W_{d} measured with a diamagnetic loop, and (g) a total neutron emission rate S_{n}. The perp. P-NB and the tang. P-NB are injected from t = ~3.5 sec. The plasma parameters such as the $\bar{n}_{\mathrm{e}}$ and the W_{d} become almost stationary after t = ~4.5 sec. The S_{n} significantly increases just after the NB injection and reach its flat top, indicating that the DD fusion reactions begin to increase due to the NB injection.

Figure 3 shows the time evolution of the frequency spectrum of the electromagnetic and/or electrostatic fluctuation measured with the ICRF antenna strap (#1) in the same discharge as that in Fig. 2. The dotted and dashed lines indicate harmonic cyclotron frequencies for D ion lf_{cD} (l = 1, 2, 3) and ^{3}He ion $l'f_{\mathrm{c3He}}$ (l' = 1, 2), respectively. These cyclotron frequencies were calculated with the magnetic field strength at the edge of the plasma on the midplane on the low field side. Currents flowing in the magnetic field coils are already constant during the

time range of Fig. 3. Namely, the temporal changes of the lf_{cD} and $l'f_{c3He}$ are due to the behaviors of the positions of the plasma edge as shown in Fig. 2(c). A strong fluctuation appears at the frequency just below the 2 f_{c3He} after the S_n begins to increase. The time variation of the frequency of the observed fluctuation is similar to that of the 2 f_{c3He}. This observed fluctuation is interpreted as the second harmonic ICE(^{3}He). Although the mechanism is not understood, only harmonic ICEs(^{3}He) are often observed while the fundamental one is not observed on JT-60U.[6] The difference in the frequency between the 2 f_{c3He} and the second harmonic ICE(^{3}He) can be mainly caused by the Doppler shift, which is discussed in section 4. The second harmonic ICE(^{3}He) continues being observed during the stationary phase. A fluctuation observed in the frequency around the f_{cD} is the fundamental ICE(D). However, we do not discuss the dispersion model for the ICE(D) to focus on the ICE(^{3}He) in this paper.

Radial profiles of electron density and temperature were measured at t = 5.1 sec. Figure 4 shows radial profiles of (a) the safety factor q, (b) the electron density n_e and (c) the electron temperature T_e at t = 5.1 sec in E48461. The q profile indicates that the magnetic shear is positive. We calculated the slowing down time τ_s of the DD fusion produced ^{3}He ions in the center of the plasma at t = 5.1 sec by using the n_e and T_e in Fig. 4. The τ_s is about 0.3-0.4 sec. The velocity distribution of the fast ^{3}He ions is also almost stationary around t = 5.1 sec because the enough longer time than the τ_s elapses after the S_n becomes constant. Hence, we used the plasma parameters in Fig. 4 for the orbit calculations to evaluate the distribution in the stationary phase. A radial profile of the ion temperature T_i is assumed to be equal to that of the T_e shown in Fig. 4(c) since the T_i profile was not measured around t = 5.1 sec in E48461 and no large difference between the T_e and the T_i was observed in other discharges where the plasma parameters are similar to those at t = 5.1 sec in E48461.

3.2 Setup for calculation of the velocity distribution

The fast ^{3}He ions are produced by the DD fusion reactions. A birth profile of the ^{3}He ions is necessary for the orbit calculations of the fast ^{3}He ions. In order to obtain the birth profile, we calculated the orbits of the fast D ions originated from the NB injections. Figure 5(a) shows a schematic drawing of the NB lines on the R-Z plane at t = 5.1 sec in E48461. Here, R is the major radius, and Z is the vertical coordinate. The solid and dashed arrows indicate the lines of the perp. P-NB and the tang. P-NB, respectively. The perp. P-NB is injected from #14 NB unit (P_{NB} =1.87 MW and E_{AC} = 80.9 kV), and the tang. P-NB from #9 NB unit (1.76

MW, 79.7 kV). The proportions of the accelerated D neutral atoms of energies E_{AC}, $E_{\mathrm{AC}}/2$, and $E_{\mathrm{AC}}/3$ are 78%, 15%, and 7%, respectively. Figure 5(b) shows a schematic drawing of sampling boxes for the evaluations of the fast ^{3}He ion velocity distribution at R = 3.53 m (dashed box), R = 4.25 m (dotted box) and 4.42 m (solid box) in the same Z positions as the magnetic axis. The lengths of the sampling boxes are 0.2 m in the Z direction and 0.08 m in the R direction. The R position of the magnetic axis is ~3.53 m. The outermost magnetic surface on the midplane on the low field side is located at R = ~4.425 m. Hence, the distributions at R = 3.53 m, 4.25 m and 4.42 m indicate the typical cases at the magnetic axis, near and at the plasma edge, respectively.

The OFMC code traces the guiding-center and/or gyro-full orbits of the fast ions in three-dimensional magnetic fields.[17] The OFMC code is validated in terms of loss and confined fast ions by comparisons of heat loads and beam driven currents with JFT-2M[18], JT-60U[19-21] and DIII-D[22] experiments. Orbit calculation conditions of the fast D ions with the OFMC code in this paper are as follows. The number of test particles is 0.1 million in order to sufficiently obtain reproducibility of the orbit calculations with the OFMC code. The test particles are followed along their guiding-center orbits until they hit the first wall or until their energies become lower than 1.25 times of the bulk ion temperature. We assumed the toroidal symmetry and neglected the magnetic ripples. The spatial distribution of the beam-thermal DD fusion produced ^{3}He ions in the stationary phase was calculated by integrating the time evolution of the product of the beam-thermal DD fusion cross section and the test particle weights until all test particles lose.

Figure 6 shows the calculated birth profile of the ^{3}He ions on the R-Z plane at t = 5.1 sec in E48461. This birth profile consists of the beam-thermal and thermal-thermal DD fusion produced ^{3}He ions. We used the birth profile in Fig. 6 for the initial positions of the test particles in the calculations of the fast ^{3}He ion orbits.

3.3 Evaluation of the velocity distribution

The fast ^{3}He ion orbits were calculated under the same condition as the case of the fast D ion except for that the number of the test particle is 0.5 million to evaluate the distribution around the plasma edge. As mentioned above, we used the birth profile in Fig. 6 for the initial positions of the test particles as the fast ^{3}He ion source. We assumed that the ^{3}He ions produced by the DD fusions are isotropic in the velocity space and have the birth energies E_{birth} (0.82 MeV).

Figure 7 shows E-ϕ_{pitch} distributions of the fast ^{3}He ions $f(E, \phi_{\mathrm{pitch}})$ at (a) R = 3.53 m

(at the magnetic axis), (b) 4.25 m (near the plasma edge) and (c) 4.42 m (at the plasma edge) at t = 5.1 sec in E48461 (see Fig. 5). Here, E and ϕ_{pitch} are energies and pitch angles of the fast ^{3}He ions, respectively. The mesh grid numbers of E and ϕ_{pitch} are 100 from 0 to 1000 keV and 180 from 0 to 180 degree, respectively. The fast ^{3}He ions distribute in relatively low E region and a width of ϕ_{pitch} is broad at R = 3.53 m. In the case of R = 4.25 m, the ϕ_{pitch} width is narrow in high E region. However, most of the fast ^{3}He ions are located in relatively low E region and there is no inverted population. On the other hand, the inversed population is formed in high E region in the case of R = 4.42 m. Additionally, the width of ϕ_{pitch} is narrow there, indicating that this distribution has strong anisotropy. Namely, the distribution in the case of R = 4.42 m has the inverted population and strong anisotropy. This is because the fast ions with the pitch angles near the trapped-passing boundary draw large trajectories and their trajectory scales become small when they are decelerated due to the ion-electron collisions. In addition, the critical energy where ion-ion collision becomes dominant in the collision process is about one hundred keV at the center of the plasma. Hence, pitch angle scatterings due to the ion-ion collisions in relatively high E region unlikely occur since their energies are sufficiently higher than the critical energy. As we mentioned in section 1, the drifting-ring-type distribution also has the inverted population and strong anisotropy. The distribution in the case of R = 4.42 m can be reasonably approximated by the drifting-ring-type distribution.

Figure 8 shows the guiding-center orbits of the fast ^{3}He ions passing through the sampling box of R = 4.42 m without the collisional effects on the R-Z plane. The orbits were calculated by using the OFMC code. The solid and dashed lines indicate the orbits of the fast ^{3}He ions having $E = E_{\mathrm{birth}}$ and $E_{\mathrm{birth}}/2$, respectively. The ϕ_{pitch} of these ions is set to 56 degree at the center of the sampling box of R = 4.42 m, since the largest populations of the fast ^{3}He ions having $E = E_{\mathrm{birth}}$ and $E_{\mathrm{birth}}/2$ in the distribution at R = 4.42 m are located around ϕ_{pitch} = 56 degree as shown in Fig. 7(c). The ^{3}He ions drawing the large banana orbit such as those in Fig. 8 contribute to the formation of the inverted population at the plasma edge.

Figure 9 shows a R position dependence of the averaged gradient of the fast ^{3}He ion distribution $\overline{\mathrm{d}f(E)/\mathrm{d}E}$ from $E = E_{\mathrm{birth}}/2$ to $E = \sim E_{\mathrm{birth}}$. Here, the $f(E)$ is the distribution as a function of only E of the fast ^{3}He ions (the energy distribution) and was calculated by integrating the $f(E, \phi_{\mathrm{pitch}})$ in the ϕ_{pitch} direction. Positive $\overline{\mathrm{d}f(E)/\mathrm{d}E}$ is located in R > ~4.39 m. This result implies that the formation of the inverted population is localized at the plasma edge.

4. Comparison of the dispersion model with the experimental observation

As we mentioned in section 1, the dispersion model using the drifting-ring-type distribution has been proposed from the several reports.[2,3,12)] In addition, the evaluated distribution at the plasma edge has the inverted population and strong anisotropy as shown in Fig.7(c), and can be reasonably approximated by the drifting-ring-type distribution. Then, we compared the dispersion model using the drifting-ring-type distribution of Eq. (1) with the experimental observation of the ICE(^{3}He) in several discharges. Here, we used the calculation model for homogeneous hot bulk D plasma including minority fast ^{3}He ions as a local approximation. We substituted thermal-Maxwellian velocity distributions and the drifting-ring-type distribution of Eq. (1) for the arbitrary velocity distribution f_0 in Eq. (10-48) of Ref. 23, and solve the wave equation of Eq. (1-27) of Ref. 24.

We evaluated the dispersions of the MCI driven by the drifting-ring-type distribution under the maximum linear growth rate condition. This maximum linear growth rate condition was obtained by searching a real wavenumber space with estimated plasma parameters at the plasma edge in the experiments. We assumed the density ratio of the fast ^{3}He ions to the bulk plasma is 10^{-4}, the bulk plasma temperature is 300 eV and $v_{||\mathrm{s}} = 0.01 v_{3\mathrm{He}}$. Here, $v_{3\mathrm{He}}$ is the speed of the fast ^{3}He ions ~7.2×10^6 m/sec which corresponds to E_{birth}. The assumptions on these parameters have little effect on the following evaluation of the dispersion. The pitch angle of the fast ^{3}He ions is expressed by $\phi_{\mathrm{pitch}} = \tan^{-1}(u/v_{||\mathrm{c}})$. The ϕ_{pitch} is set to the pitch angle where the population in the fast ^{3}He ion distribution at the plasma edge is the largest.

Figure 10 shows comparisons of (a) toroidal wavenumbers $k_{||}$ and (b) wave angular frequencies ω normalized by ^{3}He ion cyclotron angular frequencies ω_{c3He} of the calculated MCI driven by the drifting-ring-type distribution (Calc.) with those of the observed ICEs(^{3}He) (Exp.). Negative $k_{||}$ indicates that the ICE(^{3}He) propagates in the counter direction to the plasma current. The ω_{c3He} is calculated with the magnetic field strength at the edge of the plasma on the midplane on the low field side. The error bars of the $\omega/\omega_{\mathrm{c3He}}$ are small well. The circles and squares indicate the fundamental and the second harmonic ICEs(^{3}He), respectively. It is shown that the $k_{||}$ of the calculated MCIs is almost consistent with that of the observed ICEs(^{3}He) in a range of ± 1 m^{-1}. In addition, the $\omega/\omega_{\mathrm{c3He}}$ of the calculated MCIs is close to that of the observed ICEs(^{3}He). Hence, it is found that the $k_{||}$ and the $\omega/\omega_{\mathrm{c3He}}$ of the calculated MCIs agree with those of the observed ICEs(^{3}He).

The observed frequencies of the ICEs(^{3}He) are often slightly lower than the ^{3}He ion cyclotron frequencies at the plasma edge on JT-60U as shown in Fig. 3 and 10(b). The frequency based on the dispersion model of the MCI is consistent with the experimental observation as shown in Fig. 10(b). According to the theoretical analysis, the Doppler-shifted ion cyclotron resonance condition is the key to the excitation of the MCI.[9-16] The simple Doppler-shifted ^{3}He ion cyclotron resonance condition is expressed by,

$$\omega - k_{\|} V - l\omega_{\mathrm{c3He}} = 0 . \qquad (2)$$

where l is positive integer and V is a parallel velocity of the fast ^{3}He ion to the magnetic field line. The term of $k_{||}V$ indicates the Doppler shift. If the term of $k_{||}V$ is negative, the ω is lower than the $l\omega_{\mathrm{c3He}}$ according to Eq. (2). In the experiments, the $k_{||}$ is negative as shown in Fig. 10(a) and the V is positive since the pitch angle near the passing-trapped boundary is between 0 and 90 degree at the plasma edge, indicating that the term of $k_{||}V$ is negative. Hence, the cause for the difference in the frequency between the ω and the $l\omega_{\mathrm{c3He}}$ in the experiment is considered to be the Doppler shift.

5. Summary

In this paper, we compared the dispersion model of the MCI driven by the drifting-ring-type distribution with the experimental observation of the ICE(^{3}He) on JT-60U. First, the velocity distributions of the DD fusion produced fast ^{3}He ions at the time of the appearance of the ICE(^{3}He) were evaluated by using the OFMC code under the realistic condition. The results show that the distribution near the center of the plasma has no inverted population and weak anisotropy. On the other hand, the inverted and strong anisotropic distribution is formed at the edge of the plasma on the midplane on the low field side. This distribution at the plasma edge can be reasonably approximated by the drifting-ring-type distribution. Next, we compared the toroidal wavenumber and the frequency based on the model with those of the experimental observation. The dispersions based on the model were calculated under the maximum linear growth rate condition. The comparison results show that these toroidal wavenumbers are almost consistent in a range of ± 1 m^{-1} and these frequencies agree. Namely, the dispersion model of the MCI driven by the drifting-ring-type distribution is consistent with the experimental observation of the ICE(^{3}He) on JT-60U.

We are planning on an extension of the fast ion distribution function used for the dispersion model from the drifting-ring-type one to the arbitrary one in order to directly evaluate the model using the calculated distribution. In addition, investigations of the distribution which

can excite the ICE by comparison with the case when the ICE is not observed, and evaluations of the dispersions of the ICE(D), the ICE(H) and the ICE(T) are also future works.

Acknowledgement

The authors are grateful to the JT-60 team of the National Institutes for Quantum and Radiological Science and Technology for their collaboration.

Reference list

*E-mail: sumida_shuhei@prc.tsukuba.ac.jp

1) G. A. Cottrell, V. P. Bhatnagar, O. Da Costa, R. O. Dendy, J. Jacquinot, K. G. McClements, D. C. McCune, M. F. F. Nave, P. Smeulders, and D. F. H. Start, Nucl. Fusion, **33**, 1365 (1993).
2) S. Cauffman, R. Majeski, K. G. McClements, and R. O. Dendy, Nucl. Fusion, **35**, 1597 (1995).
3) K. G. McClements, C. Hunt, R. O. Dendy, and G. A. Cottrell, Phys. Rev. Lett., **82**, 2099 (1999).
4) H. Kimura, Y. Kusama, M. Saigusa, G. J. Kramer, K. Tobita, M. Nemoto, T. Kondoh, T. Nishitani, O. Da Costa, T. Ozeki, T. Oikawa, S. Moriyama, A. Morioka, G. Y. Fu, C. Z. Cheng, and V. I. Afanas'ev, Nucl. Fusion, **38**, 1303 (1998).
5) M. Ichimura, H. Higaki, S. Kakimoto, Y. Yamaguchi, K. Nemoto, M. Katano, M. Ishikawa, S. Moriyama, and T. Suzuki, Nucl. Fusion, **48**, 035012 (2008).
6) M. Ichimura, M. Katano, Y. Yamaguchi, S. Sato, Y. Motegi, H. Muro, T. Ouchi, S. Moriyama, M. Ishikawa, K. Shinohara, Y. Sakamoto, A. Kojima, and T. Watanabe, Proc. 22nd IAEA Fusion Energy Conf, Geneva, Switzerland, 2008, EX/P8-2.
7) S. Sato, M. Ichimura, Y. Yamaguchi, M. Katano, Y. Imai, T. Murakami, Y. Miyake, T. Yokoyama, S. Moriyama, T. Kobayashi, A. Kojima, K. Shinohara, Y. Sakamoto, T. Watanabe, H. Hojo, and T. Imai, Plasma Fusion Res., **5**, S2067 (2010).
8) K. Saito, R. Kumazawa, T. Seki, H. Kasahara, G. Nomura, F. Shimpo, H. Igami, M. Isobe, K. Ogawa, K. Toi, M. Osakabe, M. Nishiura, T. Watanabe, S. Yamamoto, M. Ichimura, T. Mutoh, and LHD Experiment Group, Plasma Sci. Technol., **15**, 209 (2013).
9) R. O. Dendy, C. N. Lashmore-Davies, and K. F. Kam, Phys. Fluids B, **4**, 3996 (1992).
10) R. O. Dendy, C. N. Lashmore-Davies, and K. F. Kam, Phys. Fluids B, **5**, 1937 (1993).
11) R. O. Dendy, C. N. Lashmore-Davies, K. G. McClements, and G. A. Cottrell, Phys. Plasmas, **1**, 1918 (1994).
12) K. G. McClements, R. O. Dendy, C. N. Lashmore-Davies, G. A. Cottrell, S. Cauffman, and R. Majeski, Phys. Plasmas, **3**, 543 (1996).
13) T. Fülöp, Ya. I. Kolesnichenko, M. Lisak, and D. Anderson, Nucl. Fusion, **37**, 1281 (1997).
14) T. Fülöp and M. Lisak, Nucl. Fusion, **38**, 761 (1998).
15) L. Carbajal, R. O. Dendy, S. C. Chapman, and J. W. S. Cook, Phys. Plasmas, **21**, 012106

(2014).
16) L. Carbajal, R. O. Dendy, S. C. Chapman, and J. W. S. Cook, Phys. Rev. Lett., **118**, 105001 (2017).
17) K. Tani, M. Azumi, H. Kishimoto, and S. Tamura, J. Phys. Soc. Jpn., **50**, 1726 (1981).
18) K. Shinohara, H. Kawashima, K. Tsuzuki, K. Urata, M. Sato, H. Ogawa, K. Kamiya, H. Sasao, H. Kimura, S. Kasai, Y. Kusama, Y. Miura, K. Tobita, O. Naito, the JFT-2M Group, and D. S. Darrow, Nucl. Fusion, **43**, 586 (2003).
19) K. Tobita, K. Tani, Y. Kusama, T. Nishitani, Y. Ikeda, Y. Neyatani, S. V. Konovalov, M. Kikuchi, Y. Koide, K. Hamamatsu, H. Takeuchi, and T. Fujii, Nucl. Fusion, **35**, 1585 (1995).
20) T. Oikawa, Y. Kamada, A. Isayama, T. Fujita, T. Suzuki, N. Umeda, M. Kawai, M. Kuriyama, L. R. Grisham, Y. Ikeda, K. Kajiwara, K. Ushigusa, K. Tobita, A. Morioka, M. Takechi, T. Itoh, and JT-60 Team, Nucl. Fusion, **41**, 1575 (2001).
21) K. Shinohara, S. Sakurai, M. Ishikawa, K. Tsuzuki, Y. Suzuki, K. Masaki, O. Naito, K. Kurihara, T. Suzuki, Y. Koide, T. Fujita, Y. Miura, and the JT-60 Team, Nucl. Fusion, **47**, 997 (2007).
22) G. J. Kramer, A. McLean, N. Brooks, R. V. Budny, X. Chen, W. W. Heidbrink, T. Kurki-Suonio, R. Nazikian, T. Koskela, M. J. Schaffer, K. Shinohara, J. A. Snipes, and M. A. Van Zeeland, Nucl. Fusion, **53**, 123018 (2013).
23) T. H. Stix, *Waves in Plasmas* (Springer-Verlag, New York, 1992) Chap. 10, p. 255.
24) T. H. Stix, *Waves in Plasmas* (Springer-Verlag, New York, 1992) Chap. 1, p. 8.

Figure captions

- **Figure 1.** (Color online) A schematic drawing of the ICRF antennas on JT-60U. Two antenna straps and four antenna straps are arranged in the poloidal and toroidal directions, respectively.

- **Figure 2.** (Color online) Temporal evolution of (a) a plasma current I_{P}, (b) a safety factor at 95% of the toroidal magnetic flux q_{95}, (c) a major radial position of the edge of the plasma on the midplane on the low field side R_{edge}, (d) powers P_{NB} of the perp. P-NB (solid line) and the tang. P-NB (dotted line), (e) a line-averaged density $\bar{n}_{\mathrm{e}}$, (f) a stored energy W_{d}, and (g) a total neutron emission rate S_{n} in E48461.

- **Figure 3.** (Color online) Temporal evolution of the frequency spectrum measured with the ICRF antenna strap (#1) in E48461. The harmonics of the cyclotron frequencies for D ion f_{cD} (dotted lines) and ^{3}He ion f_{c3He} (dashed line) at the edge of the plasma on the midplane on the low field side are plotted. A strong fluctuation at the frequency slightly below 2 f_{c3He} is interpreted as the second harmonic ICE(^{3}He).

- **Figure 4.** (Color online) Radial profiles of (a) the safety factor q, (b) the electron density n_{e}, and (c) the electron temperature T_{e} at t = 5.1 sec in E48461. Here, ρ is a normalized minor radius.

- **Figure 5.** (Color online) Schematic drawings of (a) #14 perp. P-NB (solid arrow) and #9 tang. P-NB (dashed arrow) lines on the R-Z plane at t = 5.1 sec in E48461, and (b) sampling boxes for the evaluations of typical fast ^{3}He ion velocity distributions. The centers of the sampling boxes are located at R = 3.53 m (dashed box), 4.25 m (dotted box) and 4.42 m (solid box) in the same Z positions as the magnetic axis. The size of the sampling boxes is 0.2 m in the Z direction and 0.08 m in the R direction.

- **Figure 6.** (Color online) The birth profile of the ^{3}He ions on the R-Z plane at t = 5.1 sec in E48461. The dotted line indicates the outermost magnetic surface.

- **Figure 7.** (Color online) E-ϕ_{pitch} distributions of the fast ^{3}He ions $f(E, \phi_{\mathrm{pitch}})$ at (a) R

= 3.53 m, (b) 4.25 m and (c) 4.42 m at t = 5.1 sec in E48461 (see Fig. 5).

- **Figure 8.** (Color online) Guiding-center orbits of the fast ^{3}He ions passing through the sampling box of R = 4.42 m without the collisional effects on the R-Z plane. The solid and dashed lines indicate the orbits of the fast ^{3}He ions having $E = E_{\mathrm{birth}}$ and $E_{\mathrm{birth}}/2$, respectively. The ϕ_{pitch} of the fast ^{3}He ions is set to 56 degree at the center of the sampling box of R = 4.42 m. The dotted line indicates the outermost magnetic surface.

- **Figure 9.** (Color online) A major radial R profile of the averaged gradient of the fast ^{3}He ion energy distribution $\overline{\mathrm{d}f(E)/\mathrm{d}E}$ from $E = E_{\mathrm{birth}}/2$ to $E = \sim E_{\mathrm{birth}}$ at t = 5.1 sec in E48461.

- **Figure 10.** (Color online) Comparisons of (a) the toroidal wavenumbers $k_{||}$ and (b) the normalized angular frequencies $\omega/\omega_{\mathrm{c3He}}$ of the calculated MCIs driven by the drifting-ring-type distribution (Calc.) with the experimental observations of the fundamental (circles) and the second harmonic (squares) ICEs(^{3}He) (Exp.). The dashed lines are plotted where the observations and the calculations are equal.

Figures

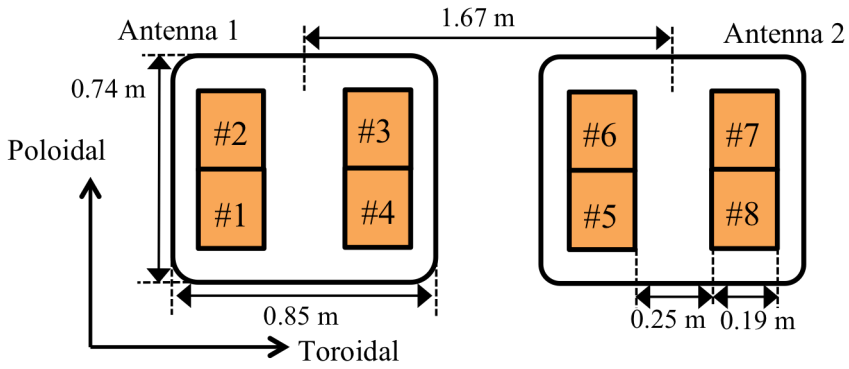

Fig. 1. (Color online) A schematic drawing of the ICRF antennas on JT-60U. Two antenna straps and four antenna straps are arranged in the poloidal and toroidal directions, respectively.

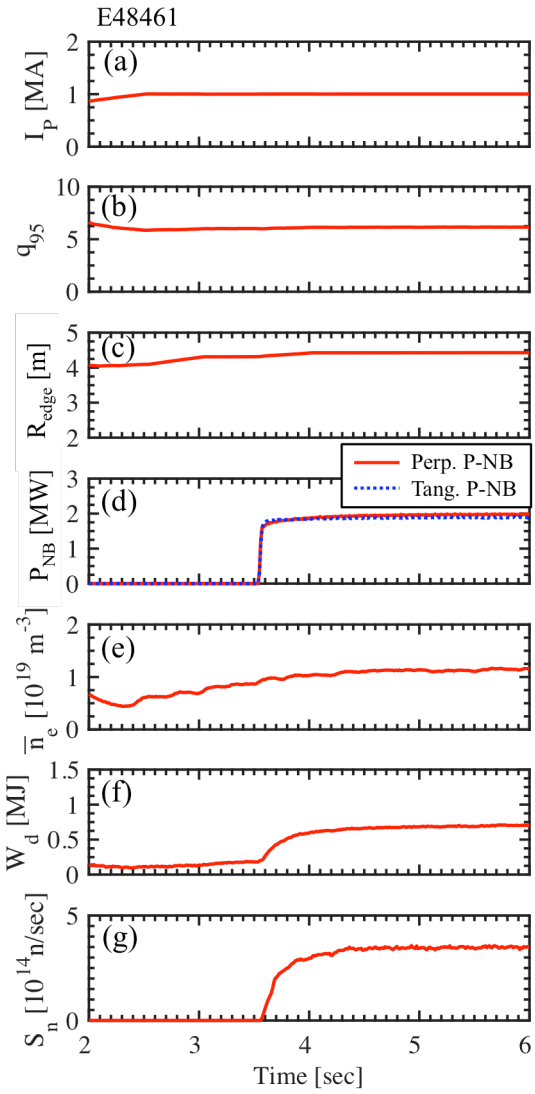

Fig. 2. (Color online) Temporal evolution of (a) a plasma current I_{P}, (b) a safety factor at 95% of the toroidal magnetic flux q_{95}, (c) a major radial position of the edge of the plasma on the midplane on the low field side R_{edge}, (d) powers P_{NB} of the perp. P-NB (solid line) and the tang. P-NB (dotted line), (e) a line-averaged density $\bar{n}_{\mathrm{e}}$, (f) a stored energy W_{d}, and (g) a total neutron emission rate S_{n} in E48461.

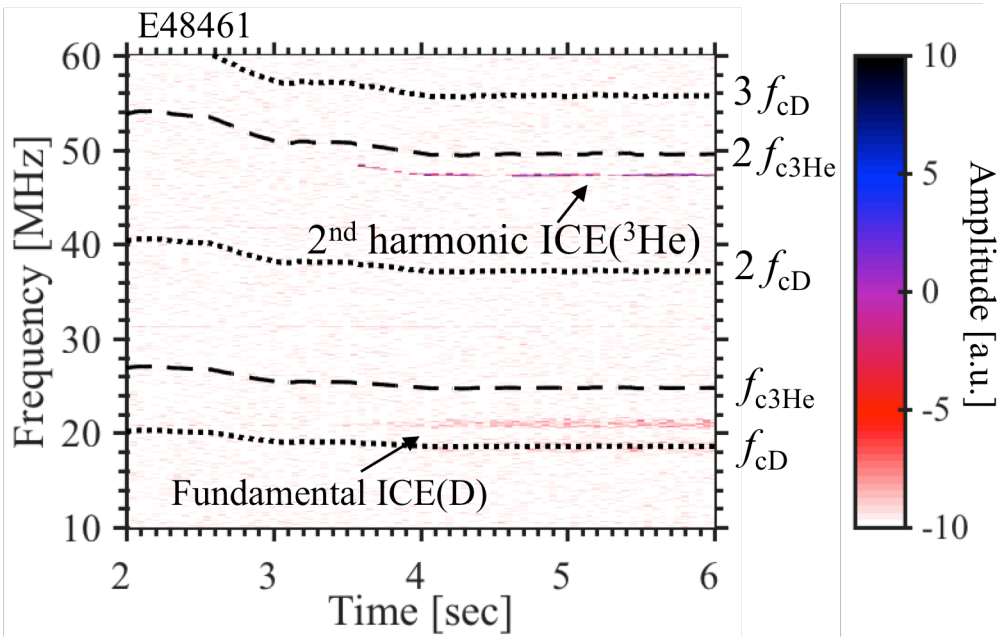

Fig. 3. (Color online) Temporal evolution of the frequency spectrum measured with the ICRF antenna strap (#1) in E48461. The harmonics of the cyclotron frequencies for D ion f_{cD} (dotted lines) and ^{3}He ion f_{c3He} (dashed line) at the edge of the plasma on the midplane on the low field side are plotted. A strong fluctuation at the frequency slightly below 2 f_{c3He} is interpreted as the second harmonic ICE(^{3}He).

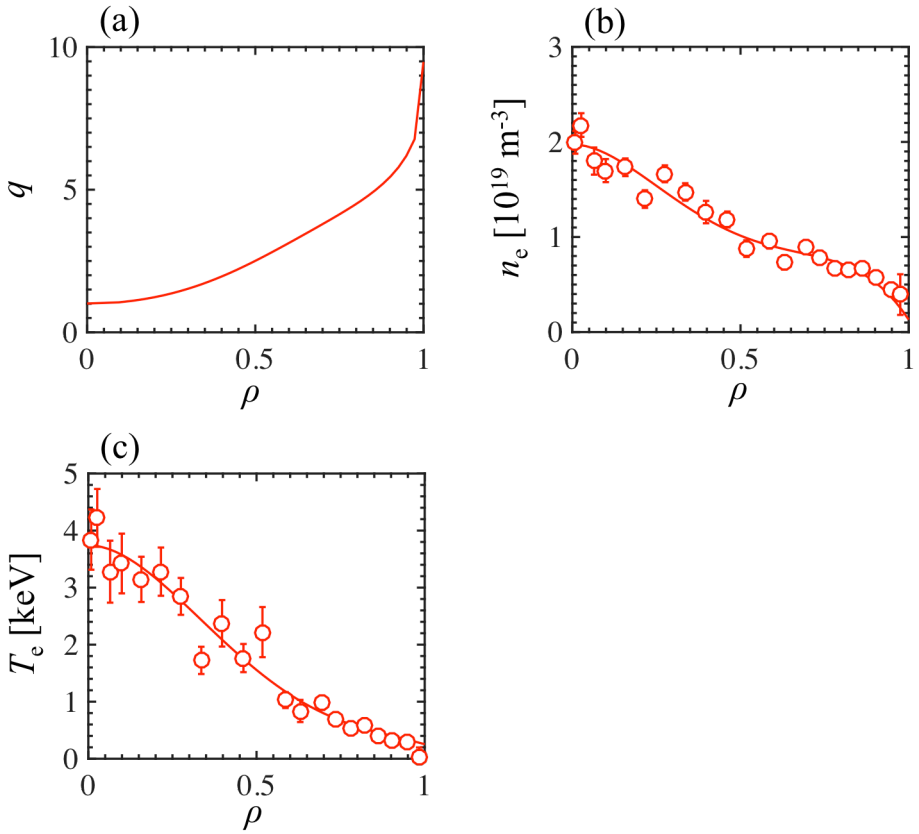

Fig. 4. (Color online) Radial profiles of (a) the safety factor q, (b) the electron density n_e, and (c) the electron temperature T_e at $t = 5.1$ sec in E48461.

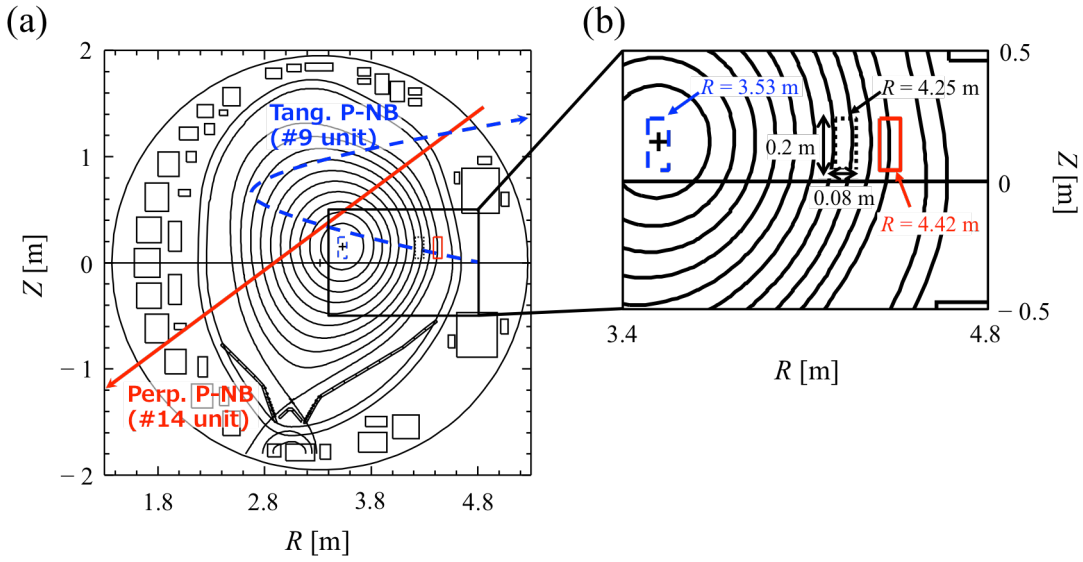

Fig. 5. (Color online) Schematic drawings of (a) #14 perp. P-NB (solid arrow) and #9 tang. P-NB (dashed arrow) lines on the *R*-*Z* plane at t = 5.1 sec in E48461, and (b) sampling boxes for the evaluations of typical fast ^{3}He ion velocity distributions. The centers of the sampling boxes are located at R = 3.53 m (dashed box), 4.25 m (dotted box) and 4.42 m (solid box) in the same Z positions as the magnetic axis. The size of the sampling boxes is 0.2 m in the Z direction and 0.08 m in the R direction.

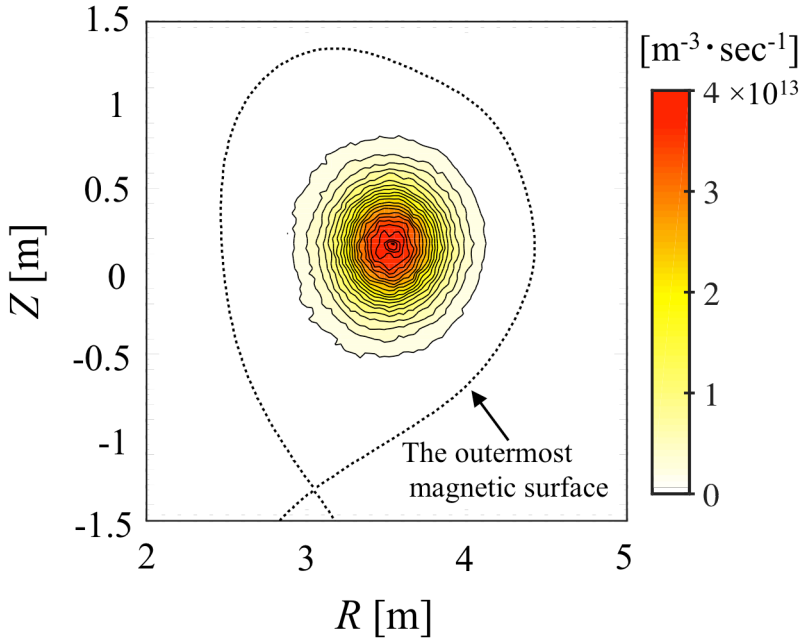

Fig. 6. (Color online) The birth profile of the ^{3}He ions on the *R*-*Z* plane at $t = 5.1$ sec in E48461. The dotted line indicates the outermost magnetic surface.

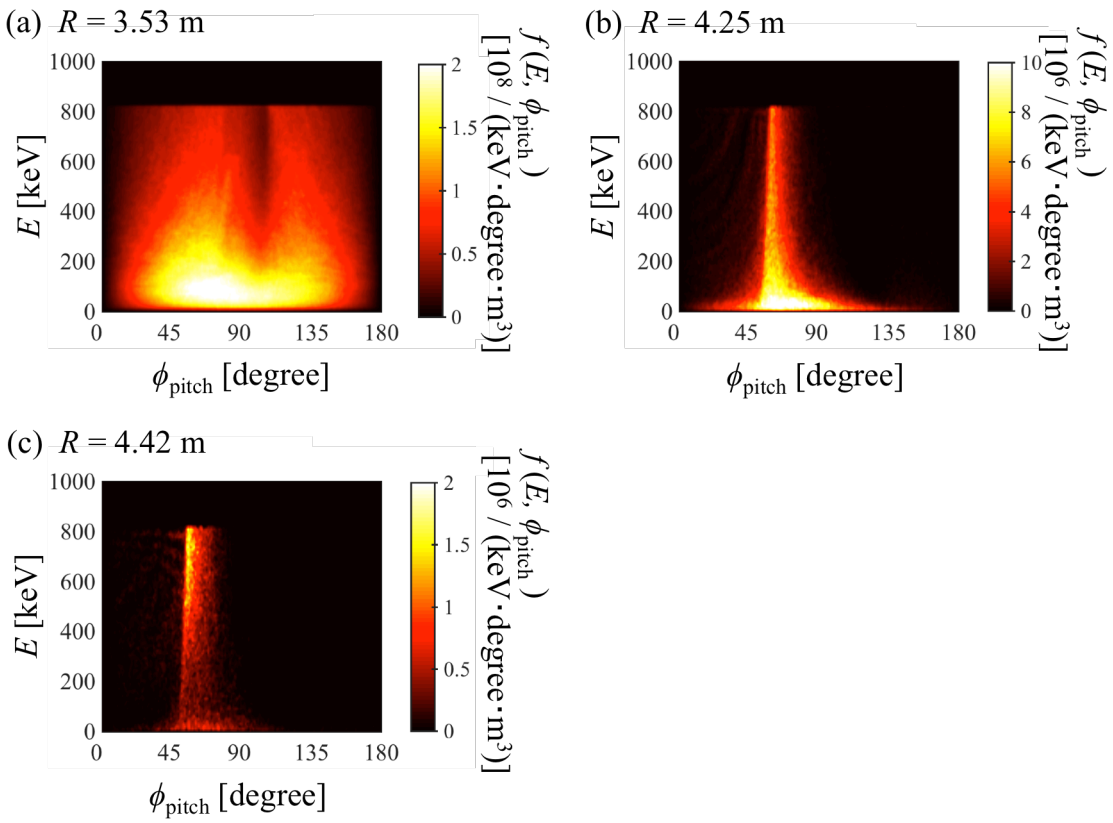

Fig. 7. (Color online) E-ϕ_{pitch} distributions of the fast ^{3}He ions $f(E, \phi_{\mathrm{pitch}})$ at (a) R = 3.53 m, (b) 4.25 m and (c) 4.42 m at t = 5.1 sec in E48461 (see Fig. 5).

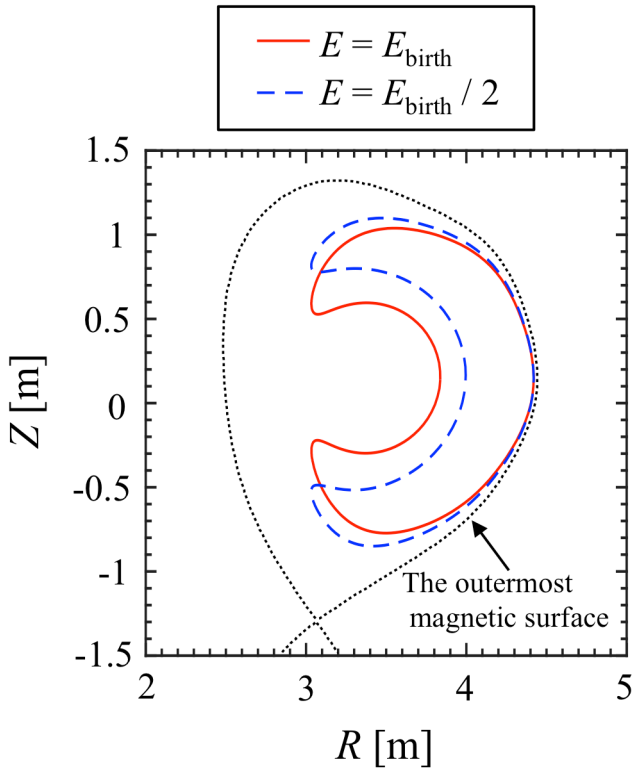

Fig. 8. (Color online) Guiding-center orbits of the fast ^{3}He ions passing through the sampling box of R = 4.42 m without the collisional effects on the R-Z plane. The solid and dashed lines indicate the orbits of the fast ^{3}He ions having $E = E_{\mathrm{birth}}$ and $E_{\mathrm{birth}}/2$, respectively. The ϕ_{pitch} of the fast ^{3}He ions is set to 56 degree at the center of the sampling box of R = 4.42 m. The dotted line indicates the outermost magnetic surface.

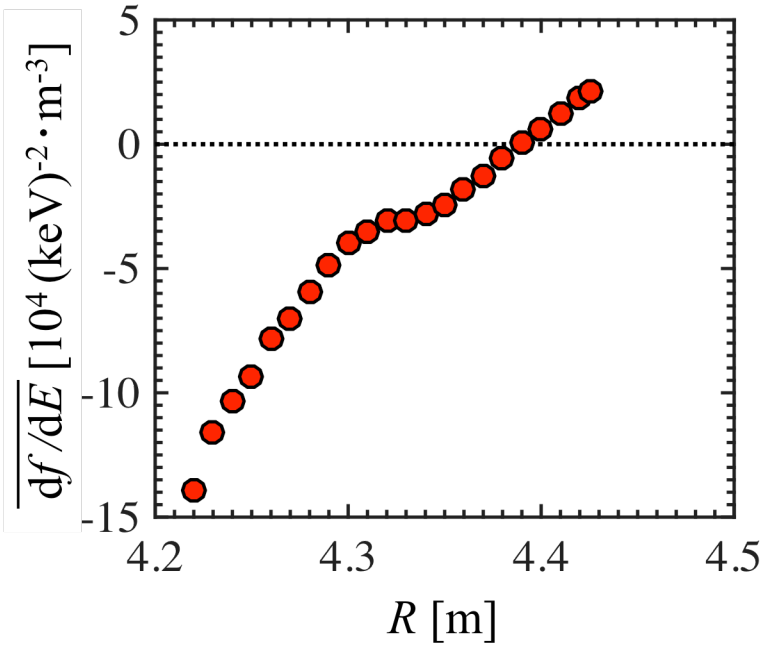

Fig. 9. (Color online) A major radial R profile of the averaged gradient of the fast ^{3}He ion energy distribution $\overline{df(E)/dE}$ from $E = E_{\mathrm{birth}}/2$ to $E = \sim E_{\mathrm{birth}}$ at t = 5.1 sec in E48461.

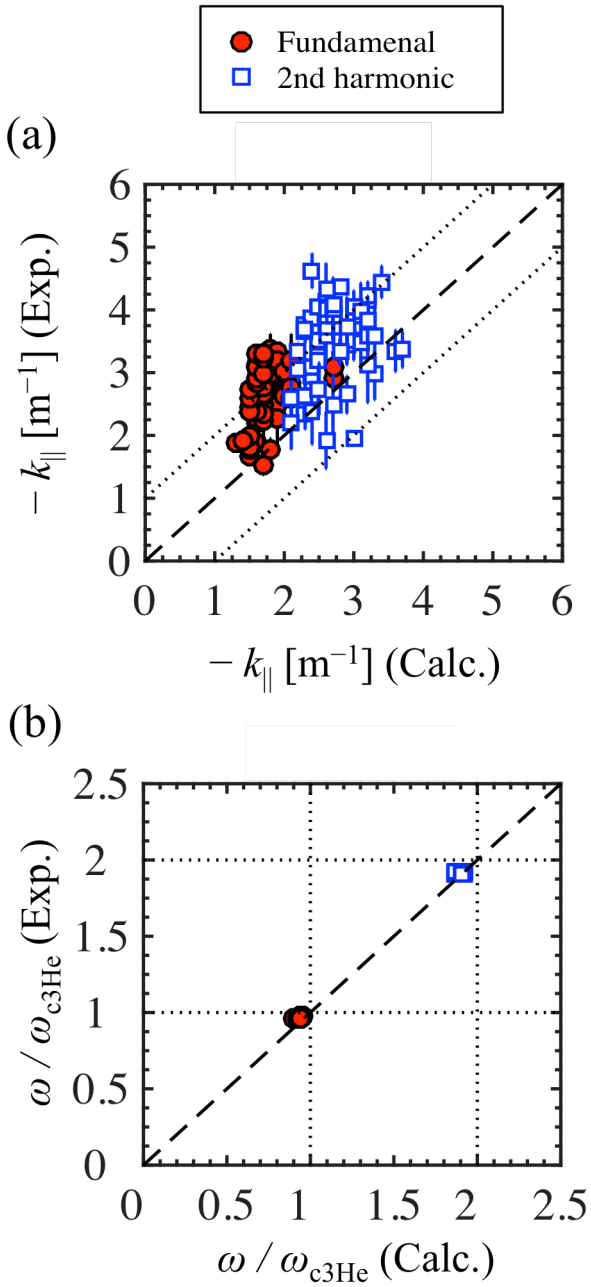

Fig. 10. (Color online) Comparisons of (a) the toroidal wavenumbers $k_{||}$ and (b) the normalized angular frequencies ω/ω_{c3He} of the calculated MCIs driven by the drifting-ring-type distribution (Calc.) with the experimental observations of the fundamental (circles) and the second harmonic (squares) ICEs(^{3}He) (Exp.). The dashed lines are plotted where the observations and the calculations are equal.